Available online at www.sciencedirect.com
SCIENCE DIRECT®
Journal of the European Ceramic Society 25 (2005) 1167–1173
www.elsevier.com/locate/jeurceramsoc

Evaluation of microstructural evolution in thermal barrier coatings during thermal cycling using impedance spectroscopy

S.-H. Song [a,*], P. Xiao [b], L.-Q. Weng [c]

[a] *Division of Materials Science and Engineering, Shenzhen Graduate School, Harbin Institute of Technology, Shenzhen University Town, Xili, Shenzhen 518055, China*
[b] *Manchester Materials Science Centre, University of Manchester, Grosvenor Street, Manchester M17HS, UK*
[c] *School of Materials Science and Technology, Nanjing University of Aeronautics and Astronautics, Nanjing 210016, China*

Received 22 February 2004; received in revised form 12 May 2004; accepted 15 May 2004
Available online 22 July 2004

Abstract

Air plasma sprayed thermal barrier coatings are thermally cycled in air up to 1030 °C and evaluated using impedance spectroscopy in conjunction with scanning electron microscopy. When the number of cycles is less than 15, impedance measurements cannot be used to detect the thermally grown oxide (TGO, usually alumina) scale because it does not fully cover the top coat-bond coat interface and the YSZ (yttria-stabilised zirconia used as the top coat) is much more electrically conductive than the alumina, leading to most of the current passing through the YSZ rather than the alumina. After the specimens are subjected to 100 until 250 cycles, impedance measurements show that a continuous alumina scale is formed. In the impedance spectra, there are four relaxation processes, which correspond to the YSZ grains, the YSZ grain boundaries, the TGO, and the electrode effect. Impedance analyses demonstrate that the resistance of the alumina scale increases and the capacitance decreases with increasing cycling. When the specimen is subjected to 400 cycles, the impedance response to the continuous TGO vanishes due to the TGO degradation.

Keywords: Thermal barrier coatings; Non-destructive evaluation; Interfaces; Electrical properties; Impedance; ZrO_2; Al_2O_3

1. Introduction

Thermal barrier coatings (TBCs) are widely used in gas turbines for propulsion and power generation.[1–6] They are thermally insulating materials with sufficient thickness and durability so as to sustain a high temperature gradient between the load-bearing alloy substrate and the coating surface. Lowering the temperature of the metal substrate extends the life of metal components. Therefore, TBCs have increasingly been employed in gas turbine engine components like blades and vanes.

A typical TBC system is composed of an oxidation-resistant alloy bond coat (usually MCrAlY, M = Ni and/or Co, and ~100–150 μm thick) on the Ni-base superalloy component and a heat-insulating ceramic top coat (usually 8 wt.% Y_2O_3-stabilised ZrO_2, i.e., YSZ, and ~200–250 μm thick) attached to the bond coat. During high temperature operation, the two coats are to be sandwiched by a thermally grown oxide (TGO, usually alumina) layer.

The mechanisms of coating failure are strongly dependent on the interfacial and microstructural features of the bi-material system.[7,8] These features evolve during high-temperature operation or thermal cycling of the system, leading to crack nucleation and propagation due to high internal stress formation and relaxation induced by both TGO growth and thermal expansion mismatch between the ceramic coating and the alloy substrate.[8–12] In our previous studies,[11,13] we have investigated the microstructural evolution of a TBC system during high temperature exposure without thermal cycling. The aim of the present work is to evaluate the microstructural evolution in a TBC system during thermal cycling using impedance spectroscopy along with scanning electron microscopy (SEM). Impedance spectroscopy is a non-destructive evaluation technique in ceramic material research.[14] The principle of the technique is to relate the

* Corresponding author. Tel.: +86 755 26033801; fax: +86 755 26033732.
E-mail address: shsonguk@yahoo.co.uk (S.-H. Song).

0955-2219/$ – see front matter © 2004 Elsevier Ltd. All rights reserved.
doi:10.1016/j.jeurceramsoc.2004.05.007

electrical properties of the material to its microstructural features.[11,15–17]

2. Experimental procedure

Specimens with a coating area of 20 mm × 20 mm were prepared by air plasma spraying (APS) with both a bond coat (~150 μm thick) and a top coat (~250 μm thick) on Haynes-230 superalloy plates (3 mm thick). The chemical composition of the superalloy (wt.%) is 22 Cr, 14 W, 3 Fe, 2 Mo, 0.02 La, 0.015 B, and 0.1 C with nickel in balance. Chemical composition of the bond coat alloy (wt.%) is 32 Ni, 38.5 Co, 21 Cr, 8 Al, and 0.5 Y. The YSZ contains 8 wt.% Y_2O_3 and 92 wt.% ZrO_2. The specimens were thermally cycled as shown in Fig. 1. In each cycle, the specimens well maintained at 200 °C were heated to 1030 °C at a rate of 8 K/min, held there for 1 h, and then cooled to 850 °C at a rate of 10 K/min, then to 650 °C at a rate of 5 K/min, and finally to 200 °C at a rate of 3 K/min. Three specimens were used for each thermal cycling condition.

For impedance measurements, the metal side of the oxidised specimen was mechanically polished to remove the oxide layer and acted as one electrode. The TBC side was coated with a silver paint in an area of 64 mm^2, which served as the other electrode. In order to consolidate the silver paint and enhance its adhesion to the specimen surface, the paint was cured at 400 °C for 30 min. Impedance measurements were conducted at 400 °C using a Solartron SI 1255 HF frequency response analyser coupled with a Solartron 1296 Dielectric Interface, which is computer-controlled. Spectra analysis (fitting) was performed using Zview impedance analysis software (Scribner Associates Inc., Southern Pines, NC) to obtain the electrical properties of TBCs. In the measurements, an AC (alternating current) amplitude of 100 mV was employed and the AC frequency was in the range of 1 × 10^{-4} Hz to 1 × 10^{7} Hz. The measured results were represented by the mean values of data points obtained along with the standard deviation.

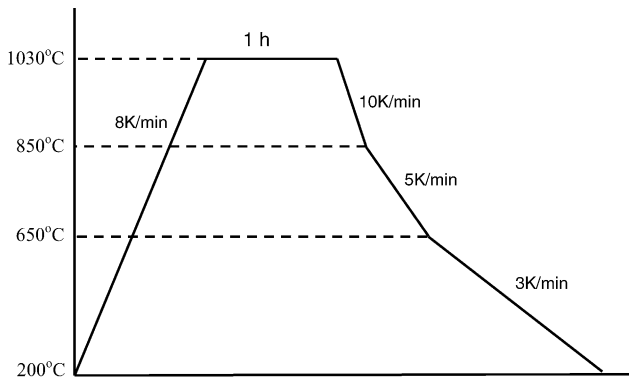

Fig. 1. Schematic diagram showing the procedure of thermal cycling.

Microstructures of the specimens were examined by the use of a JEOL 6300 scanning electron microscope equipped with a LINKS energy dispersive X-ray microanalyser (EDX).

3. Results and discussion

3.1. Microstructure

The cross sections of the thermally cycled specimens are shown in Fig. 2. In the specimen subjected to 15 cycles, a TGO layer was formed but it is not continuous. After 100-cycle treatment, a continuous TGO layer was formed at the bond coat/top coat interface. The thickness of the TGO layer increases with increasing cycling number and its morphology exhibits no apparent change until 250 cycles. However, after 400 cycles there is no apparent increase in the thickness of the TGO layer but in some regions the black TGO has changed to the grey TGO. As for the YSZ, there appears to be more cracks in the more cycled specimens. The EDX analyses indicate that the black TGO mainly contains Al and O with the amount of Cr, Co, Ni, and Y less than 1 at.%, but the grey one contains about 10 at.% Cr, 7 at.% Co, 2 at.% Ni, and 1 at.% Y in addition to Al and O. As a consequence, the black TGO should be Al_2O_3 while the grey one could be a mixture of Al_2O_3, (Ni,Co)Al_2O_4, NiO, CoO, and Cr_2O_3. This has also been confirmed elsewhere.[12,18–20] Many cavities have been formed in the grey oxide area (Fig. 2d). Owing to the fact that the thermal cycling creates internal stresses due to both TGO growth and YSZ-metal thermal expansion misfit.[7,8,21,22] It can be envisaged that these cavities would enlarge and coalesce to each other with the thermal cycling going on so as to form cracks. This is in conformity to the work by Ali et al.[12] where it was found that the cracks initiated and propagated within the grey mixed oxide layer, leading to the spallation of the YSZ top coat for a plasma-sprayed TBC system.

As described in Ref. 8, initially the Al activity in the bond coat is very high and the formation of Al_2O_3 is dominant. Whenever the alumina is stable, the O activity at the interface is too low to form other oxides. Upon the alumina growth, the Al activity decreases due to its depletion while the O activity increases at the interface. When the O activity at the interface reaches a certain level, the Al_2O_3 converts to $NiAl_2O_4$ through the reaction: $3Ni + 4Al_2O_3 = 3NiAl_2O_4 + 2Al$. In the case of NiCoCrAlY alloy bond coat, the spinel should be (Ni,Co)Al_2O_4. Furthermore, when the O activity at the interface increases, the solubilities of Ni, Co and Cr in the alumina also increases. In such an instance, Ni, Co and Cr in the bond coat could move to cross the bond coat-TGO boundary into the TGO and thus a concentration gradient of Ni, Co and Cr could be established between the inner and outer surfaces of the TGO. This concentration gradient would cause outward diffusion of cations (Ni, Co and Cr ions) through the TGO. Upon meeting higher O activities, these cations may form new oxides like Cr_2O_3 and NiO, and

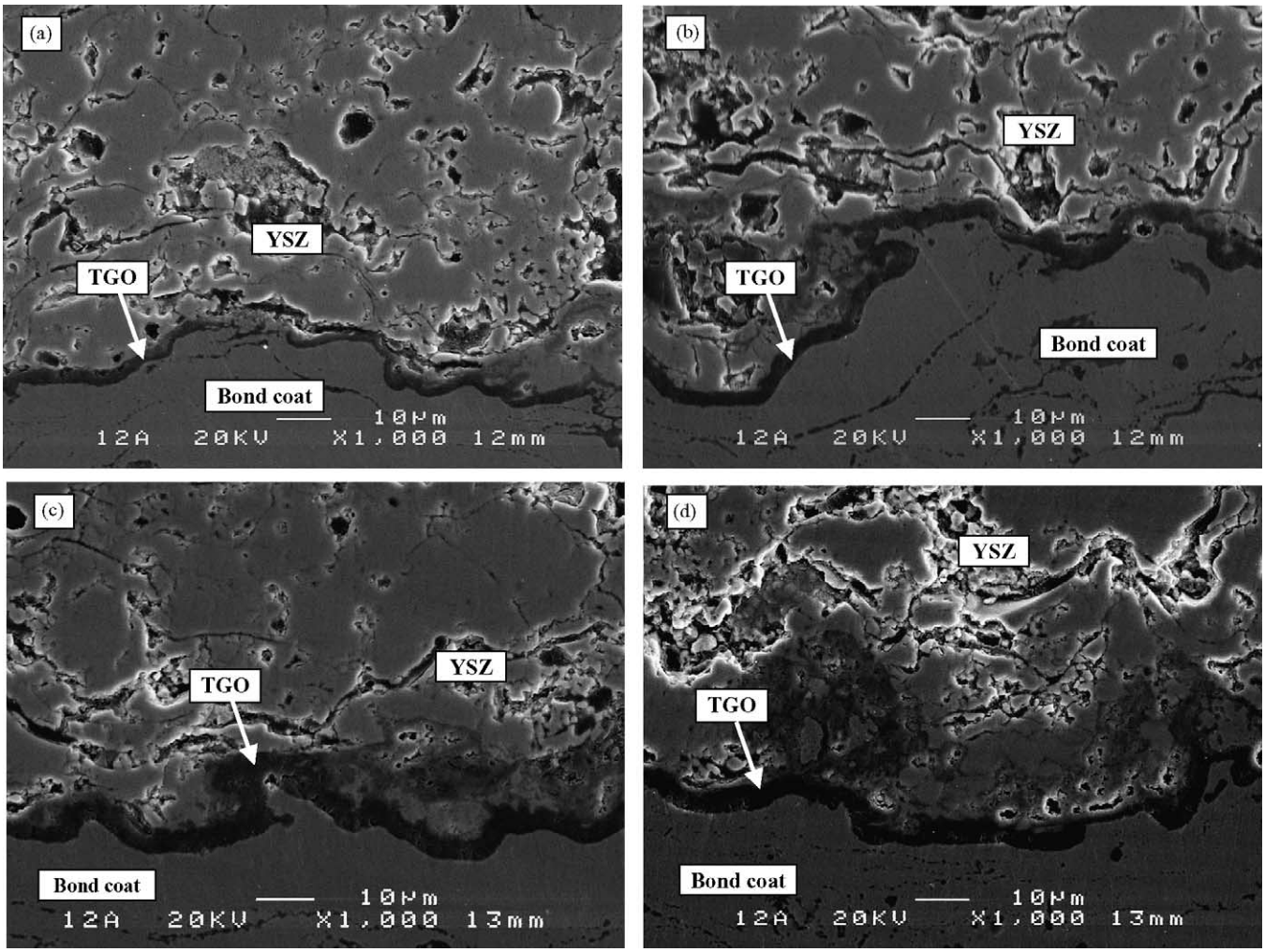

Fig. 2. Scanning electron micrographs showing the cross sections of different thermally cycled TBC specimens: (a) 15 cycles; (b) 100 cycles; (c) 250 cycles; and (d) 400 cycles.

Ni or Co cations may cause the conversion of the alumina to the spinel in regions between the TGO and the YSZ. In the present work, there is no apparent spinel present between the bond coat and the alumina but there are apparent mixed oxides present between the alumina and the YSZ. The reason for the former may be that the O activity at the former is not high enough to cause the alumina-to-spinel conversion.

3.2. Electrical properties and their relation to microstructural features

Impedance measurements for different specimens have been conducted using impedance spectroscopy. There are different presentations of impedance data, in which Nyquist and Bode plots are most frequently used.[14] In a Nyquist plot, the impedance is represented by a real part Z' and an imaginary part Z'' with the formula $Z(\omega) = Z' + jZ''$, where ω is the angular frequency and $j = \sqrt{-1}$. In a Bode plot, the modulus of the impedance and the phase angle are both plotted as a function of frequency. For a simple resistor–capacitor (R–C) circuit, the Nyquist plot is characterised by a single semicircle. However, for a multi-R–C circuit (a multilayer system formed by different materials), the Nyquist plot would consist of several semicircles that may partially overlap to each other. Usually, the Nyquist plot is used to determine the major parameters, such as resistance and capacitance corresponding to an electrochemical system by fitting the measured spectra according to an equivalent circuit, which corresponds to a physical model of the system. As described in Refs. 13,14,23, for an oxide scale system, the measured capacitance response is often not ideal, i.e., not a pure capacitor. This deviation can be modelled by the use of a constant phase element (CPE) instead of an ideal capacitance element in the equivalent circuit. The impedance of a CPE, Z_{CPE}, is given by[14,15,23]

$$Z_{\mathrm{CPE}} = \frac{1}{A(j\omega)^n} \tag{1}$$

where A is a parameter independent of frequency. When the exponential factor $n = 1$, the CPE functions as an ideal ca-

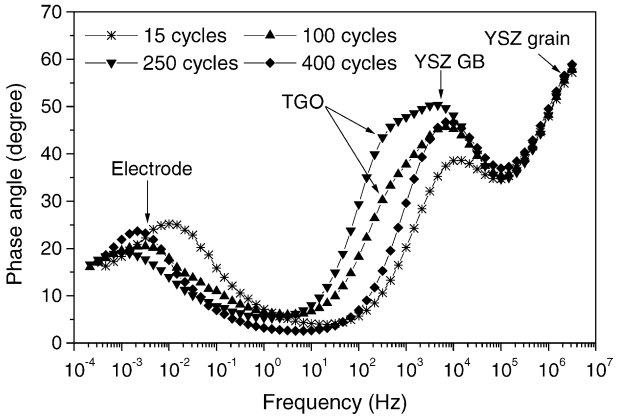

Fig. 3. Phase angle as a function of frequency for the different thermally cycled specimens.

pacitor and A is therefore equal to the capacitance C. In most cases, n is less than 1. In general, a CPE is associated with chemical inhomogeneity and geometrical non-uniformity, which cause a frequency dispersion.[23] In the case of no ideal capacitive response, the value of A cannot be used to represent the capacitance of the system. Here we adopt an equivalent capacitance C, which may be acquired by[24]

$$C = R^{(1-n)/n} A^{1/n} \quad (2)$$

where R is the resistance.

The phase angles are represented in Fig. 3 as a function of frequency. There are three relaxation processes (characterised by inflections) for the specimens subjected to 15 and 400 cycles while there are four for the specimens subjected to 100 and 250 cycles. For all the specimens, the highest or second highest frequency relaxation has a similar relaxation frequency. It has been confirmed[13,25,26] that the lowest frequency relaxation stems from the electrode effect rather than the material being investigated and the highest and second highest frequency relaxations are the responses from the grains and grain boundaries of the YSZ, respectively. The third relaxation process from the right-hand side, which may be seen for the specimens subjected to 100 and 250 cycles although it is not very clear, originates from a continuous thermally grown alumina layer. The typical relaxation frequency for the alumina layer is about 300 Hz. Therefore, the presence of the discontinuous thermally grown oxide layer should be the reason for not having this relaxation process in the specimen subjected to 15 cycles (Fig. 2a). This is because the YSZ is much more conductive than the TGO and thus the current is conducted almost through the non-TGO areas rather than the TGO areas at the metal–YSZ interface so that there is no response from the TGO. However, if the chemical composition changes in the alumina or a mixed oxide layer (which comprises alumina, chromia, spinel, nickel oxide, etc.) is formed at the metal–YSZ interface, making the TGO less insulating than the pure alumina, the third relaxation process may overlap with the YSZ grain boundary response. In this case, the second highest frequency relaxation is a combined effect from YSZ grain boundaries and mixed oxides.[13,25,26] This should be the reason why the specimen subjected to 400 cycles does not exhibit the third relaxation process in the phase angle–frequency plot as the TGO has undergone some change from alumina to mixed oxides. As a consequence, the disappearance of the third relaxation frequency is an indication that the TGO has degraded from a continuous alumina layer to a mixed oxide layer. As for the cracks in the YSZ, it is difficult to detect its change by impedance measurements unless the cracking is so severe that an interface across the specimen is formed. This is because the YSZ is very conductive compared with the cracks so that most of the current can pass through the YSZ rather than through the cracks, leading to no response from the cracks. The present case could be like this.

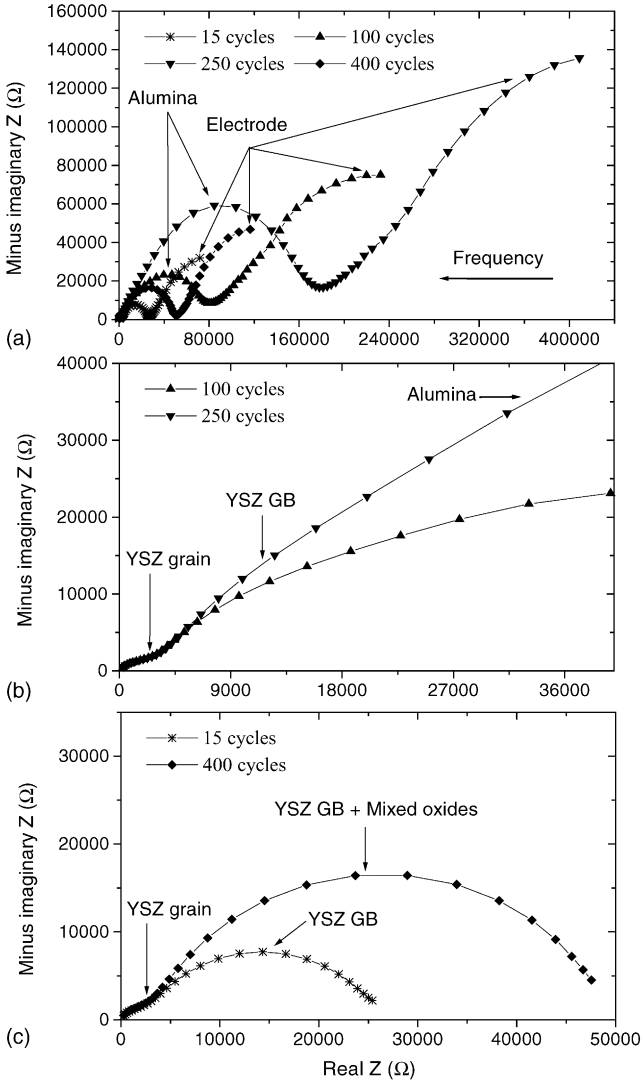

Fig. 4. Nyquist impedance plots for different thermally cycled specimens. Panels (b) and (c) show the high frequency range in panel (a).

Typical Nyquist plots for different thermally cycled specimens are represented in Fig. 4. With the exception of the electrode effect characterised by the tail in the low frequency

range, the overall resistance, which is represented by the intercept on the real impedance axis,[14] increases sharply from 15 cycles to 100 cycles and then to 250 cycles. However, after the specimen is subjected to 400 thermal cycles, it falls down considerably to the value slightly greater than that for the specimen subjected to 15 cycles. Moreover, including the electrode effect, there are three semicircles (arcs) for the specimens subjected to 15 and 400 cycles and four for the specimens subjected to 100 and 250 cycles. In the Nyquist plot, the frequency increases from the right-hand side to the left-hand side. With reference to the phase angle–frequency plot (Fig. 3), the three semicircles (arcs) are the responses from the YSZ grains, the YSZ grain boundaries and the continuous alumina layer, respectively, for the specimens subjected to 100 and 250 cycles. Clearly, the diameters of the semicircles corresponding to the alumina layer are far larger than those corresponding to the YSZ grains and grain boundaries, indicating that the resistance is much larger for the alumina than for the others. Since the TGO does not fully cover the metal–YSZ interface in the specimen subjected to 15 cycles and has degraded in composition and microstructure in the specimen subjected to 400 cycles, there are just two semicircles (arcs) present in the Nyquist plots. It is worth mentioning that the second semicircle (arc) should arise from a combined effect of YSZ grain boundaries and mixed oxides for the specimen subjected to 400 cycles but just from YSZ grain boundaries for the specimen subjected to 15 cycles (Fig. 4c).

To obtain the electrical properties of different layers, we have fitted the measured spectra (Nyquist plots) using an equivalent circuit model together with Zview impedance analysis software (Scribner Associates Inc, Southern Pines, NC). Details of the fitting procedure have been described in detail elsewhere.[13] In brief, except for the electrode effect the two semicircles in the spectra for the specimens subjected to 15 and 400 cycles can be simulated based on a model of two *R-CEP* components with a series connection, which correspond to YSZ grains and YSZ grain boundaries. The three semicircles in the spectra for the specimens subjected to 100 and 250 cycles can be simulated based on a model of three *R-CPE* components, corresponding to YSZ grains, YSZ grain boundaries, and the TGO (alumina). In the present work, the electrode effect was fitted directly using circle fitting with the above software. Of note is that the fitting itself can bring about errors, making the fitted values of the electrical properties have some difference from the actual ones. However, with the same software the fitted values should have the same trend as the actual ones, which is most concerned in this study. In the present analysis, the errors are based on the fitted values from three specimens used for each condition rather than on fitting errors.

The resistances of the YSZ grains, the YSZ grain boundaries, and the TGO are represented in Fig. 5a as a function of the number of cycles. Obviously, there is no apparent change in the resistance of YSZ grains for different specimens although they have some differences in cracks. As described earlier, it is difficult to detect the crack changes in the YSZ by impedance measurements as most of the current can pass through the YSZ rather than through the cracks, leading to no response from the cracks. For the YSZ grain boundaries, the resistance exhibits no change in the specimens subjected to up to 250 cycles, but it is increased evidently in the specimen subjected to 400 cycles. This is because, as depicted above, the latter is a combined effect from the YSZ grain boundary and the degraded TGO (mixed oxides). For the specimens subjected to 100 and 250 cycles, the resistance of the TGO increases with increasing cycles, demonstrating an increase in the thickness of the TGO as shown in Fig. 2. The capacitances of the YSZ grains, the YSZ grain boundaries, and the TGO are shown in Fig. 5b. As in the case of resistance, there is no apparent change in the capacitance of YSZ grains for different specimens. The capacitance of YSZ grain boundaries for the specimen subjected to 400 cycles is slightly decreased, indicating also again the combined effect from the YSZ grain boundaries and the degraded TGO.

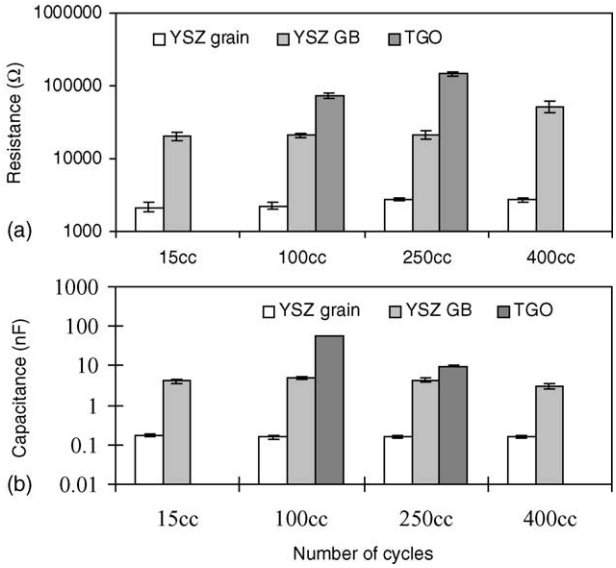

Fig. 5. The resistance and capacitance of the YSZ grains, the YSZ grain boundaries, and the TGO for different thermally cycled specimens (error bars represent the standard deviation of the fitted values; the YSZ GB resistance for the 400 cycled specimen is due to both YSZ grain boundaries and mixed oxides).

The capacitance and resistance from the electrode effect are shown in Fig. 6. Clearly, there is no apparent change in capacitance. The resistance increases with increasing cycling until 250 cycles while it decreases sharply for the specimen subjected to 400 cycles as compared to that for the specimens subjected to 100 and 250 cycles. According to Armstrong and Todd,[27] the electrode effect is from the interfaces between the silver electrode and the YSZ and between the TGO and YSZ. It has been confirmed[26] that the YSZ-TGO interface is mainly responsible for the electrode effect in a TBC system. Since the electrode effect forms a semicircle (arc), the impedance diagram is characterised by a double layer capacitance and a charge transfer resistance as shown

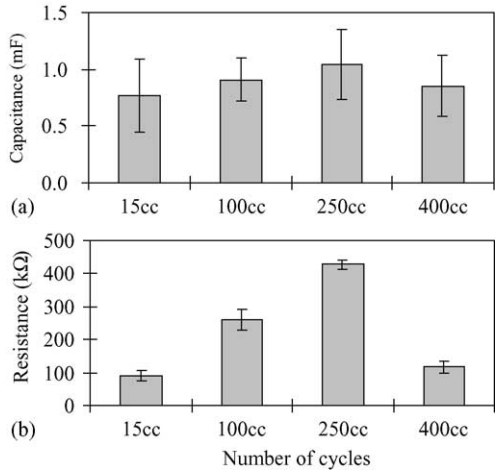

Fig. 6. The capacitance and resistance from the electrode effect from different thermally cycled specimens (error bars represent the standard deviation of the fitted values).

in Fig. 6. Owing to the fact that the capacitance for the electrode does not change for different specimens, the double layer conditions have no apparent change during thermal cycling. It is noted from Figs. 5a and 6b that the resistance from the electrode effect changes in the same order as the overall resistance from the YSZ and the TGO. As is well known, the total voltage is equal to the sum of voltages responsible for the YSZ, the TGO, and the electrode double layer, each of which is proportional to its resistance. Moreover, the linear relationship between the voltage and the charge transfer resistance or the electrode double layer thickness may not exist. Consequently, the charge transfer resistance from the electrode effect increases with decreasing voltage acted on the electrode double layer. Since this voltage decreases with increasing overall resistance of the electrolyte materials being studied, caused mainly by the TGO growth, the charge transfer resistance would increase. Therefore, the resistance from the electrode effect may be used to reflect the changes in the overall resistance of the electrolyte materials.

4. Summary

Air plasma sprayed TBCs have been thermally cycled in air up to 1030 °C and evaluated by means of impedance spectroscopy in conjunction of scanning electron microscopy. When the number of cycles is less than 15, the oxide alumina scale formed between the top and bond coats does not fully cover the top coat-bond coat interface. In this *scenario*, impedance measurements cannot be used to detect the alumina scale because the YSZ is much more electrically conductive than the alumina, leading to most of the current going through the YSZ rather than the alumina. After the specimens are subjected to 100 until 250 cycles, impedance measurements show that a continuous alumina scale is formed. In the impedance spectra, there are four relaxation processes, which correspond to the YSZ grains, the YSZ grain boundaries, the TGO, and the electrode effect. Impedance analyses demonstrate that the resistance of the alumina scale increases and the capacitance decreases with increasing cycling. This implies that the protective capability of the scale is not reduced up to 250 cycles. When the specimen is subjected to 400 cycles, the impedance response to the continuous TGO disappears because the TGO has degraded to a certain extent from alumina to mixed oxides, indicating that the protective capability of the scale is reduced. The resistance for the electrode effect changes in the same order as the overall resistance of the electrolyte materials being investigated and thus may be used to reflect changes in the overall resistance.

Acknowledgements

The authors would like to thank Professor B. Ralph of Brunel University (UK) for commenting on the manuscript.

References

1. Miller, R. A., Oxidation-based model for thermal barrier coating life. *J. Am. Ceram. Soc.* 1984, **67**, 517–521.
2. DeMasi-Marcin, J. T. and Gupta, D. K., Protective coatings in the gas-turbine engine. *Surf. Coat. Technol.* 1994, **68**, 1–9.
3. Strangman, T. E., Thermal barrier coatings for turbine airfoils. *Thin Solid Films* 1985, **127**, 93–105.
4. Meier, S. M. and Gupta, D. K., The evaluation of thermal barrier coatings in gas-turbine engine applications. *J. Eng. Gas Turbines Power—Trans ASME* 1994, **116**, 250–257.
5. Wright, P. K., Influence of cyclic strain on life of a PVD TBC. *Mater. Sci. Eng. A* 1998, **245**, 191–200.
6. Wright, P. K. and Evans, A. G., Mechanisms governing the performance of thermal barrier coatings. *Curr. Opin. Solid State Mater. Sci.* 1999, **4**, 255–265.
7. Busso, E. P., Lin, J., Sakurai, S. and Nakayama, M., A mechanistic study of oxidation-induced degradation in a plasma-sprayed thermal barrier coating system. Part I: model formulation. *Acta Mater.* 2001, **49**, 1515–1528.
8. Evans, A. G., Mumm, D. R., Hutchinson, J. W., Meier, G. H. and Pettit, F. S., Mechanisms controlling the durability of thermal barrier coatings. *Prog. Mater. Sci.* 2001, **46**, 505–553.
9. Clarke, D. R., Christensen, R. J. and Tolpygo, V., The evolution of oxidation stresses in zirconia thermal barrier coated superalloy leading to spalling failure. *Surf. Coat. Technol.* 1997, **94/95**, 89–93.
10. Sohn, Y. H., Kim, J. H., Jordan, E. H. and Gell, M., Thermal cycling of EB-PVD/MCrAlY thermal barrier coatings: 1. Microstructural development and spallation mechanisms. *Surf. Coat. Technol.* 2001, **146/147**, 70–78.
11. Ali, M. S., Song, S.-H. and Xiao, P., Evaluation of degradation of thermal barrier coatings using impedance spectroscopy. *J. Eur. Ceram. Soc.* 2002, **22**, 101–107.
12. Ali, M. S., Song, S.-H. and Xiao, P., Degradation of thermal barrier coatings due to thermal cycling up to 1150 °C. *J. Mater. Sci.* 2002, **37**, 2097–2102.
13. Song, S.-H. and Xiao, P., An impedance spectroscopy study of high-temperature oxidation of thermal barrier coatings. *Mater. Sci. Eng. B* 2003, **97**, 46–53.

14. MacDonald, J. R. (ed.), *Impedance Spectroscopy*. John Wiley & Sons, Chichester, UK, 1987.
15. Fletcher, J. G., West, A. R. and Irvine, J. T. S., The AC-impedance response of the physical interface between yttria-stabilized zirconia and $YBa_2Cu_3O_{7-x}$. *J. Electrochem. Soc.* 1995, **142**, 2650–2654.
16. Steil, M. C., Thevenot, F. and Kleitz, M., Densification of yttria-stabilized zirconia—impedance spectroscopy analysis. *J. Electrochem. Soc.* 1997, **144**, 390–398.
17. Pan, J., Leygraf, C., Jargelius-Pettersson, R. F. A. and Linden, J., Characterization of high-temperature oxide films on stainless steels by electrochemical-impedance spectroscopy. *Oxid. Met.* 1998, **50**, 431–455.
18. Murphy, K. S., More, K. L. and Lance, M. J., As-deposited mixed zone in thermally grown oxide beneath a thermal barrier coating. *Surf. Coat. Technol.* 2001, **146/147**, 152–161.
19. Belzunce, F. J., Higuera, V. and Poveda, S., High temperature oxidation of HFPD thermal-sprayed MCrAlY coatings. *Mater. Sci. Eng. A* 2001, **297**, 162–167.
20. Choi, H. S., Yoon, B., Kim, H. J. and Lee, C. H., Isothermal oxidation of air plasma spray NiCrAlY bond coatings. *Surf. Coat. Technol.* 2002, **150**, 297–308.
21. Busso, E. P., Lin, J. and Sakurai, S., A mechanistic study of oxidation-induced degradation in a plasma-sprayed thermal barrier coating system. Part II: life prediction model. *Acta Mater.* 2001, **49**, 1529–1536.
22. Haynes, J. A., Ferber, M. K., Porter, W. D. and Rigney, E. D., Mechanical properties and fracture behavior of interfacial alumina scales on plasma-sprayed thermal barrier coatings. *Mater. High Temp.* 1999, **16**, 49–69.
23. Amaral, S. T. and Muller, I. L., Effect of silicate on passive films anodically formed on iron in alkaline solution as studied by electrochemical impedance spectroscopy. *Corrosion* 1999, **55**, 17–23.
24. Jacobsen, T., Zachau-Christiansen, B., Bay, L. and Skaarup, S., SOFC cathode mechanisms. In *Proceedings of the 17th Riso Internaltional Symposium on Materials Science: High temperature Electrochemistry: Ceramics and Metals*, ed. F. W. Paulsen, N. Bonanos, S. Linderoth, M. Mogensen and B. Zachau-Christiansen. Riso National Laboratory, Roskilde, Denmark, 1996, pp. 29–40.
25. Wang, X., *Impedance Spectroscopy Evaluation of Ceramic Materials*. Ph.D. thesis, Brunel University, UK, 2001.
26. Ali, M. S., *Degradation of Thermal Barrier Coatings*. Ph.D. thesis, Brunel University, UK, 2002.
27. Armstrong, R. D. and Todd, M., *Interfacial Electrochemistry in Solid State Electrochemistry*, ed. P. G. Bruce. Cambridge University Press, Cambridge, UK, 1995.